Stainless Steel Alloys from First-principles Theory

L. Vitos, H. L. Zhang, N. Al-Zoubi, S. Lu, J.-O. Nilsson, S. Hertzman, G. Nilson, B. Johansson

Gaining an accurate description of materials obviously requires the most advanced atomic-scale techniques from both experimental and theoretical areas. In spite of the vast number of available techniques, however, the experimental study of the atomic-scale properties and phenomena even in simple solids is rather difficult. In steels the challenges become more complex due to the interplay between the structural, chemical and magnetic effects. On the other hand, advanced computational methods based on density functional theory ensure a proper platform for studying the fundamental properties of steel materials from first-principles. Our group at the Royal Institute of Technology in Stockholm has an international position in developing and applying computational codes for such applications. Using our ab initio *tools, we have presented an insight to the electronic and magnetic structure, and micromechanical properties of austenitic stainless steel alloys. In the present contribution, we review the most important developments within the* ab initio quantum-mechanics-aided steel design *with special emphasis on the role of magnetism on the fundamental properties of alloy steels.*

Keywords: First-principles theory, density functional theory, stainless steels, magnetism, stacking fault energy, elastic properties

INTRODUCTION

Today we are experiencing revolutionary changes taking place within *ab initio computational steel design*. Twenty years ago, the first-principles description of the thermodynamic properties of elemental iron was still on the borderline of atomistic simulations. However, in 2010, the Materials Research Society Fall meeting in Boston hosted for the first time a symposium focusing entirely on *Steel and Ab initio* [1]. In early 2011, the first test flights with aircrafts employing special steel alloys developed by integrated computational design based on first-principles quantum theory took place (G. B. Olson, Ref. [1]). These and numerous other application oriented activities taking place at industrial or academic sectors are paired by a clear scientific interest reflected by the number of publications *on ab initio steel research*, which has increased from null to about one thousand within the last two decades (Fig. 1). The list of the most active places boosting these changes is headed by Royal Institute of Technology Stockholm and includes reputable institutes such as Northwestern University, Belgian Nuclear Research Center, University Lille, Princeton University, or Delft University of Technology. Our research group at the Royal Institute of Technology in Stockholm has an internationally recognized position in developing and applying *ab initio* computational codes for steel related applications.

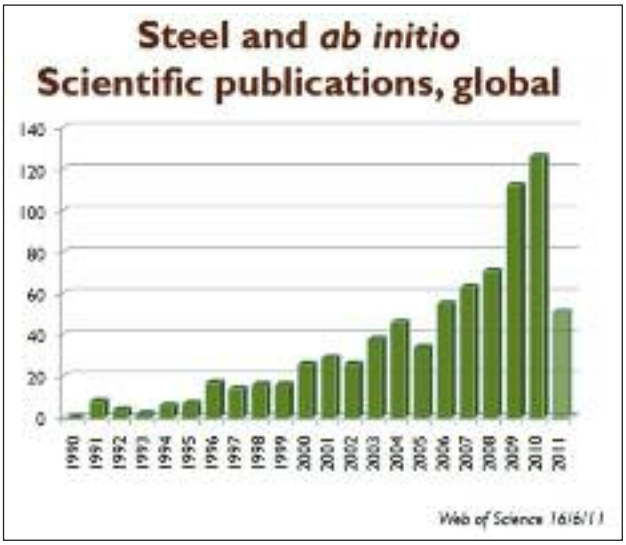

FIG. 1 ***The number of scientific (ab initio) publications on steels.***

Numero di pubblicazioni scientifiche (ab initio) sugli acciai.

Steels are mainly composed of iron and carbon. Other alloying elements are introduced in order to achieve some specific properties. The stainless steels are alloy steels containing more than

L. Vitos, H. L. Zhang, N. Al-Zoubi, S. Lu, B. Johansson
Applied Materials Physics,
Department of Materials Science and Engineering,
Royal Institute of Technology, SE-10044 Stockholm, Sweden

L. Vitos, B. Johansson
Division for Materials Theory,
Department of Physics and Materials Science,
Uppsala University, S-75120 Uppsala, Sweden

L. Vitos
Research Institute for Solid State Physics and Optics,
P.O.Box 49, H-1525 Budapest, Hungary

J.-O. Nilsson
AB Sandvik Materials Technology, SE-811 81 Sandviken, Sweden

S. Hertzman
Outokumpu Stainless Research Foundation,
Royal Institute of Technology, SE-100 44, Stockholm, Sweden
G. Nilson - Uddeholms AB, 683 85 Hagfors, Sweden

Keynote lecture presented
at the 7th European Stainless Steel Conference
Como, Italy 21-23 September 2011, organized by AIM

12 percent Cr. Chromium forms a passive film on the surface, which makes these alloys resistant against corrosion in various chemical environments [2]. Austenitic stainless steels, the largest sub-category of stainless steels, comprise a significant amount of substitutional Ni as well. At low temperatures, these alloys exhibit a rich variety of magnetic structures as a function of chemical composition, ranging from ferromagnetic phase to spin-glass and antiferromagnetic alignments. At ambient conditions, Ni changes the ferromagnetic α-Fe structure of Fe-Cr steel to the metastable paramagnetic γ-Fe structure. Today austenitic stainless steels dominate the steel applications, where excellent mechanical properties in combination with high corrosion resistance are required. The austenitic grades represent the primary choice also when non-magnetic properties are concerned.

By mechanical properties one means the behavior of materials under external load. They are of key importance both in fabrication processes and use. The behavior of materials is usually described in terms of stress or force per unit area and strain or displacement per unit distance. On the basis of stress and strain relations, one can distinguish elastic and plastic regimes. At small stress, the displacement and applied force obey the Hooke's law and the specimen returns to its original shape on unloading. Beyond the so called elastic limit, upon strain release the material is left with a permanent shape. Within the elastic regime, the elastic constants play the principal role in describing the stress-strain relation, whereas in the plastic regime the deformation induced increase in strength describes the resistance of material to permanent deformations. Plastic deformations are facilitated by dislocation motion and can occur at stress levels far below those required for dislocation-free crystals. Tensile strength may be related to the yield stress separating the elastic and plastic regions, above which a substantial dislocation activity develops. In an ideal crystal, dislocations can move easily because they experience only the weak periodic lattice potential. In real crystals, however, the motion of dislocations is impeded by obstacles, leading to an elevation of the yield strength. In particular, in solid-solutions the yield stress is decomposed into the Peierls stress needed to move a dislocation in the crystal potential and the solid-solution strengthening contribution due to dislocation pinning by the randomly distributed solute atoms. The Peierls stress of pure metals is found to be approximately proportional to the shear modulus [3]. Dislocation pinning by random obstacles is controlled by the size and elastic misfit parameters [4]. The misfit parameters, in turn, can be derived from the composition dependent elastic properties of bulk solids. The effect of alloying elements on the elastic moduli of Fe and Fe-based alloys was studied by Speich and coworkers [5] and Ghosh and Olson [6]. Many of those measurements, however, were performed on multiphase samples, and thus the obtained elastic parameters correspond to a mixed microstructure rather than to a well defined crystal structure and hence give no information about the solid-solution strengthening mechanism within a particular phase.

The formation energies of two-dimensional defects are also important in describing the mechanical characteristics of solids. An important planar defect is the stacking fault in close-packed lattices. In these structures, the dislocations may split into energetically more favorable partial dislocations having Burgers vectors smaller than a unit lattice translation. The partial dislocations are bound together and move as a unit across the slip plane. In the ribbon connecting the partials the original ideal stacking of close-packed lattice is faulted. The energy associated with this miss-packing is the stacking-fault energy (SFE). The equilibrium separation of the partial dislocations is determined by the balance of the repulsive interaction and the stacking fault energy. Generally, larger stacking fault energy corresponds to smaller distance between the partials. During the dislocation movement, the partials must re-combine in order to overcome the obstacles (e.g. solute atoms). The resistance of materials to plastic deformation decreases with increasing SFE and hence in order to increase their strength the SFE should be lowered. In solid-solutions, the stacking fault energy may be varied, whereby wider or narrower dislocations can be produced and the mechanical properties can be altered accordingly. In practice, SFE is controlled by alloying elements towards desired properties such as strength or work hardening rate. Although, the stacking fault energy in steels has been determined from experiments [7], it should be mentioned that it is difficult to measure precisely and large inaccuracies are associated with the available experimental values (see Table I).

In the present work, we review some of our recent results [7,10-16] obtained for Fe-based alloys forming the basis of stainless steels. For those readers who are familiar with density functional methods and atomistic computer simulations, in Section 1 we provide a brief overview of the employed first-principles quantum mechanical tool. The theoretical results are presented and discussed in the second chapter. Here we cover two main topics: stacking faults and elastic properties. At the end, we bring forward some fresh theoretical data on a closely related topic: alloying induced softening or hardening against tetragonal distortions.

FIRST-PRINCIPLES APPROACH

Computational method

Today there are a large number of first-principles computational tools available which can in principle be employed to study the fundamental properties of Fe-based systems. When it comes to the Fe-based solid solutions and especially to paramagnetic austenitic stainless steel alloys, the number of suitable first-principles tools is very limited. Our ability to reach an *ab initio* atomistic level approach in the case of such complex systems has become possible by the Exact Muffin-Tin Orbitals (EMTO) method. The EMTO method [17-19] is an improved screened Korringa-Kohn-Rostoker method for solving the one-electron equations within density functional theory [20]. In the EMTO approach, the one-electron potential is represented by large overlapping muffin-tin potential spheres. By using overlapping spheres, one describes more accurately the crystal potential, when compared to the conventional non-overlapping muffin-tin approach. The method is based on the Green's function and full charge density techniques [21]. The problem of disorder is treated within the coherent-potential approximation (CPA) [22,23].

In the present applications, the total charge density was obtained from self-consistent calculations based on the local density approximation for the exchange-correlation potential and the total energy was evaluated within the Perdew-Burke-Ernzerhof (PBE) generalized gradient approximation for the exchange-correlation functional [24]. The paramagnetic state of Fe alloys was simulated by the so-called disordered local moments (DLM) model [25]. Within the DLM picture, a pseudo-binary paramagnetic $Fe_{1-x}M_x$ alloy (M may stand for a group of atoms) is modeled as a quaternary $(Fe^{\uparrow}Fe^{\downarrow})_{1-x}(M^{\uparrow}M^{\downarrow})_x$ alloy with equal amount of spin-up ($^{\uparrow}$) and spin-down ($^{\downarrow}$) alloy components. In this way, the CPA Green's function corresponds to a random mixture of spin-up and spin-down atoms, and thus will automatically ensure a spin-neutral effective medium for the magnetic impurities. Therefore, even though formally the DLM calculations are performed at 0 K, the effect of the loss of the net magnetic moment above the Curie temperature on the total energy

is properly captured. The size of the disordered local magnetic moments on each atom is determined fully self-consistently without any constraint. The main approximation within this static DLM model is the neglect of the longitudinal spin fluctuations present in the paramagnetic state. Going beyond this simple CPA-based approach to describe the paramagnetic state requires taking into account the magnetic excitations as well as the thermo-elastic-magnetic coupling. Further details of the self-consistent total energy calculations presented in this contribution can be found in Refs. [7, 10-16].

During the last decade, the EMTO method was employed in the theoretical study of the properties of random Fe-based alloys [7,10-16,19], simple and transition metal alloys [19,26-28], and Hume-Rothery systems [19,23,26,29], as well as complex oxides [19,30,31]. All these applications demonstrate that the EMTO approach in combination with the CPA is an efficient tool for describing the alloying effects on the atomic-scale properties of random substitutional solid solutions. Its particular strength is that in contrast to previous CPA implementations, it is suitable to study properties and processes involving anisotropic lattice distortions or low symmetry structures. However, since the EMTO method is based on the optimized overlapping muffin-tin potential approach (that is, it uses certain shape approximation for the Kohn-Sham potential) special care must be taken when applying to open or multicomponent systems. Furthermore, owing to the single-site approximation, this method has some limitations for systems with substantial charge transfer between alloy components or when the short range order and local lattice relaxation effects become important. In order to control the above problems, each application must be preceded by a series of test calculations to find the best numerical parameters for the problem in question. This assumes well educated users who are also familiar within the complex world of the computational first-principles materials science.

Bulk parameters

The elastic properties of single crystals are described by the elements c_{ij} of the elasticity tensor. There are three independent elastic constants for a cubic lattice: c_{11}, c_{12}, and c_{44}, and they are connected to the tetragonal shear modulus $c' \equiv (c_{11}-c_{12})/2$ and the bulk modulus $B = (c_{11}+2c_{12})/3$. Dynamical (mechanical) stability requires that $c_{44} > 0$, $c' > 0$, $B > 0$. The cubic elastic constants of the paramagnetic fcc $Fe_{1-x}M_x$ (M = Cr or Co) random alloys were calculated as a function of the chemical composition for $0 \le x \le 0.1$. At each concentration x the theoretical equilibrium lattice parameter a(x) and bulk modulus B(x) were derived from an exponential Morse type function fitted to the *ab initio* total energies calculated for seven different atomic volumes (Wigner-Seitz radius, w). The two cubic shear moduli c'(x) and c_{44}(x) were computed using the volume-conserving orthorhombic and monoclinic deformations and the polycrystalline elastic moduli were obtained by the Voigt-Reuss-Hill averaging method [19].

The total energies along the Bain path for the paramagnetic Fe-Cr and Fe-Cr-Ni alloys were computed for 2.60 Bohr $\le$ w $\le$ 2.75 Bohr and $0.9 \le c/a \le 1.55$ (c/a stands for the tetragonal axial ratio). For each system, we performed calculations for seven different w and 14 different c/a ratios.

The most common stacking fault in an fcc crystal, the so-called intrinsic staking fault, may be viewed as a missing (111) layer from an otherwise perfect lattice. The excess free energy ΔF per unit interface area (A_{2D}) defines the fault energy γ. Within the axial interaction model [7], taking into account interactions between layers up to the third nearest neighbors, ΔF can be obtained from the free energies of the hexagonal close packed (hcp), double hcp (dhcp) and fcc lattices as $\Delta F = F_{hcp} + 2F_{dhcp} - 3F_{fcc}$. The temperature (T) dependent magnetic moment $\mu(T)$, representing the set of local magnetic moments, was determined from the minimum of the free energy $F(T,\mu) = E(T,\mu) - T[S_{mag}(\mu) + S_{el}(T)]$ calculated at the theoretical equilibrium volume. The electronic energy $E(T,\mu)$ and entropy $S_{el}(T)$ were obtained from spin-constrained calculations, using the finite-temperature Fermi distribution. The magnetic entropy was estimated using the mean-field expression $S_{mag}(\mu) = k_B \log(1+\mu)$ (k_B is the Boltzmann constant) valid for completely disordered localized moments. The phonon contribution to ΔF was neglected, which was estimated to introduce an error ~2 mJ/m^2 in γ [10].

WHAT FIRST-PRINCIPLES THEORY PROVIDES

Stacking fault energy

Using our first-principles methods, we have determined the SFE of Fe-Cr-Ni alloys as a function of temperature and chemical composition (Fig. 2). For a few selected compositions, the theoretical predictions are compared to the experimental data in Table I. For a more detailed comparison between the theoretical and the available experimental stacking fault energy data, including the strong temperature dependence of the SFE, the reader is referred to Refs. [7,10,11].

For the considered composition interval and for temperature of 300 K (Fig. 2a), the total stacking fault energy of austenitic steels varies between -10 mJ/m^2 corresponding approximately to $Fe_{0.66}Cr_{0.26}Ni_{0.08}$, and ~50 mJ/m^2 corresponding to $Fe_{0.66}Cr_{0.14}Ni_{0.20}$. That is, at 300 K the Cr-rich and Ni-poor alloys are unstable against the fcc-to-hcp martensitic transformation. Nickel is found to increase the stacking fault energy. However, its effect strongly depends on the amount of Cr. Namely, at low Cr content (less than 16-18 %), Ni has negligible effect on SFE in alloys containing more than ~12 % Ni. At large Cr content, on the other hand, Ni has a pronounced increasing effect on the SFE. It should be pointed out that Cr has a weak but clear nonlinear effect on the SFE for alloys containing more than ~18 % Ni.

FIG. 2
Calculated stacking fault energy (γ) of paramagnetic fcc Fe-Cr-Ni alloys plotted as a function of Ni and Cr contents for 300 K (left panel) and 0 K (right panel).
Energia di stacking fault calcolata (γ) per leghe paramagnetiche fcc Fe-Cr-Ni, tracciata in funzione dei contenuti di Ni e Cr a 300 K (sinistra) e 0 K (destra).

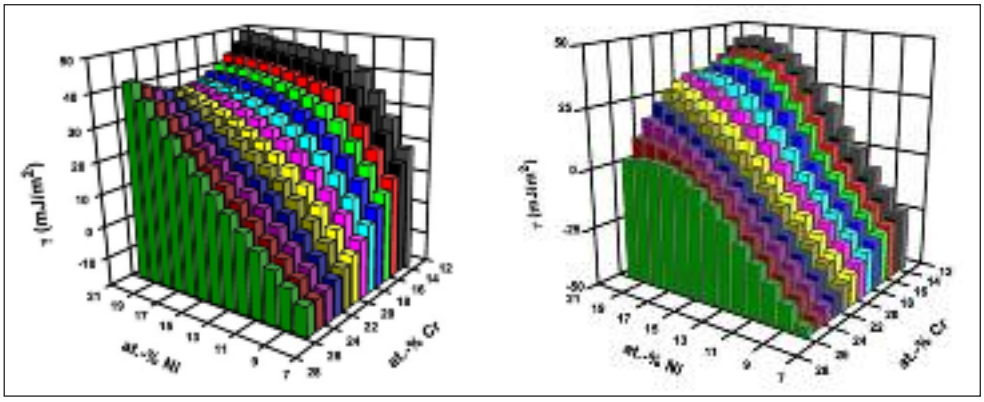

Cr	Ni	theory	experiment
15	14	40.1	46±7
17	13	30.9	23±5
17	20	38.8	31±5
19	10	11.7	7.2±1.5, 25±2.5, 16.4±1.1
22	13	18.4	18±4
26	20	42.0	40±5

TAB. I ***Comparison between the calculated and experimental [7] stacking fault energies for six selected alloys. Compositions are given in atomic percent and SFE in mJ/m².***

Confronto fra le energie di stacking fault (SFE) calculate e sperimentali [7] per sei leghe selezionate. Le composizioni sono date in percentuali atomiche e SFE in mJ/m².

From Fig. 2a, one would conclude that in general with increasing Ni content in paramagnetic Fe-Cr-Ni alloys the width of the ribbon connecting the partial dislocations decreases so that the partials can more easily recombine and thus the resistance of the alloy against plastic deformation decreases. At the same time, Cr is predicted to enhance the strength of the alloy at low Ni content and have negligible effect at large Ni content. However, the above trends show strong temperature dependence. On the right panel of Fig. 2, we show the calculated SFE at 0 K. The overall effect of Ni at 0 K is similar to that from Fig. 2a, but Cr is found to decrease the SFE at any Ni content. We will show below that the reason behind this change is the behavior of the local magnetic moment with alloying.

We find that the above chemical effects of alloying additions are accompanied by major magnetic effects, which in fact stabilize the most common industrial alloy steels at normal service temperatures. Note that according to Fig. 2b, all Fe-Cr-Ni alloys encompassing less than ~11-17 % Ni (depending on Cr content) have negative SFE at 0 K. At 300 K, only alloys within a small compositional range have still negative SFE and they are located in the low-Ni-high-Cr part of the map from Fig. 2a. Within the present model, the temperature part of the SFE corresponds mainly to the magnetic entropy contribution to the SFE. Since the local magnetic moments in the double hexagonal structure are calculated to be close to those within the fcc structure, the magnetic fluctuation part of the SFE reduces to $\gamma^{mag} = -T[S^{hcp} - S^{fcc}]/A_{2D}$ (where S stands for the magnetic plus electronic entropy and A_{2D} is the interface area). γ^{mag} is plotted in Fig. 3a for 300 K. We can observe that γ^{mag} exhibits a strongly nonlinear composition dependence, especially for low-Ni alloys (as a function of Cr content) and for high-Cr alloys (as a function of Ni content). Because at 300 K the leading term in the entropy is the magnetic contribution, the above trends are direct consequences of the composition dependence of the magnetic moments for the fcc and hcp phases [11].

We illustrate the change of the local magnetic moments in the case of $Fe_{0.68}Cr_{0.20}Ni_{0.12}$ and $Fe_{0.60}Cr_{0.20}Ni_{0.20}$ alloys. According to the axial interaction model [11], the stacking fault energy is computed from the total energies of the double hexagonal, hcp and fcc lattices. In these calculations, the atomic volume is assumed to be constant and equal to that of the parent fcc lattice. However, in real alloys due to the vanishing local magnetic moments in the hcp environment, the hcp lattice prefers a smaller equilibrium volume than that of the fcc lattice. Due to the in-plane lattice constraint volume relaxation can be realized only along the direction perpendicular to the stacking fault plane. To mimic this situation, in our calculations we relaxed the c lattice constant of the hcp lattice while keeping the in-plane lattice constant a fixed to $a_{fcc}^{(111)}$. The calculated total energies are shown in Fig. 3b (left axis) as a function of c/a. In alloys containing 12 % Ni, the hexagonal lattice is nonmagnetic (the local magnetic moments vanish within the hcp phase, see Fig. 3b right axis and also Fig.2 from Ref. [11]) and thus there should be a large volume relaxation relative to the volume of the fcc lattice. This is reflected by the very small equilibrium c/a≈1.57 obtained for hcp $Fe_{0.68}Cr_{0.20}Ni_{0.12}$ and the large γ^{mag} calculated for this alloy (Fig. 3a). When the Ni content is increased to 20 %, the hcp lattice becomes weakly magnetic (small local magnetic moments appear on Fe sites, see Fig. 3b right axis and also Fig.2 from Ref. [11]). Therefore, the equilibrium volume of hcp $Fe_{0.60}Cr_{0.20}Ni_{0.20}$ should be close to that of the fcc phase. Indeed, the calculated equilibrium c/a≈1.62 for hcp $Fe_{0.60}Cr_{0.20}Ni_{0.20}$ is very close to the ideal one (~1.63), meaning that in this alloy no substantial volume relaxation takes place around the stacking fault. In consequence, the magnetic fluctuation contribution to the stacking fault energy of $Fe_{0.60}Cr_{0.20}Ni_{0.20}$ alloys becomes very small (Fig. 3a).

The results summarized in Figs. 2 and 3 clearly demonstrate the importance of the disordered local moments for the stacking

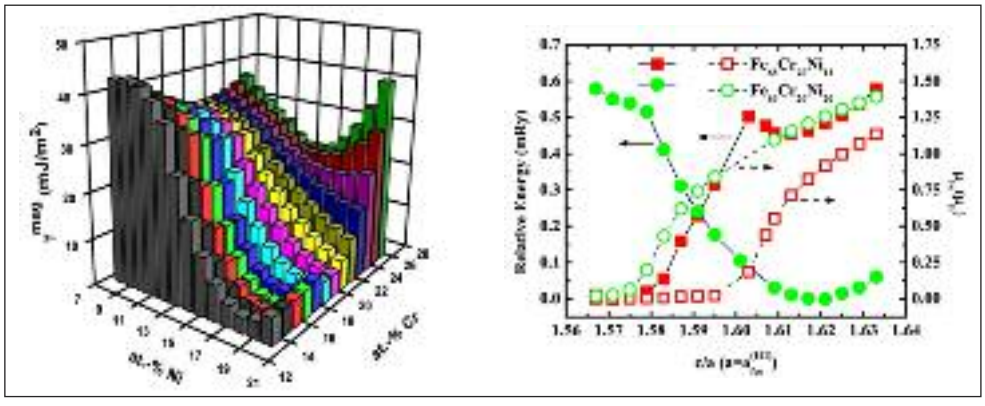

FIG. 3
a) magnetic fluctuation contribution to the stacking fault energy (mag) of fcc Fe-Cr-Ni alloys calculated for 300 K. b) total energy (left axis) and local magnetic moment (right axis) for the hcp Fe-Cr-Ni alloys as a function of hexagonal lattice parameter c/a keeping the in-plane lattice constant a fixed to that of the fcc lattice (afcc(111)). Notice the different orientations of the Ni and Cr axes on Fig. 2 and Fig. 3a.

a) contributo della fluttuazione magnetica all'energia di stacking fault (mag) di leghe fcc Fe-Cr-Ni calcolato a 300 K. b) energia totale (asse sinistro) e momento magnetico locale (asse destro) per le leghe hcp Fe-Cr-Ni in funzione del parametro del reticolo esagonale c/a, mantenendo la costante a del reticolo planare fissa rispetto a quella del reticolo fcc (afcc(111)). Si noti il diverso orientamento degli assi Ni e Cr riportati nelle Fig. 2 e Fig. 3a.

FIG. 4
Calculated stacking fault energy maps of Fe-Cr-Ni-Mn (a) and Fe-Cr-Ni-Co (b) alloys plotted as a function of composition for T = 300 K.

Mappe dell'energia di stacking fault calcolata per leghe Fe-Cr-Ni-Mn (a) e Fe-Cr-Ni-Co (b) tracciate in funzione della composizione per T = 300 K.

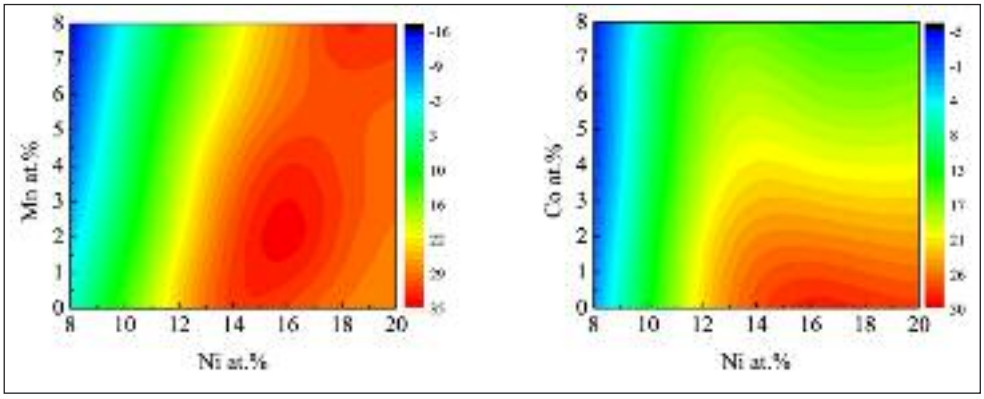

FIG. 5
Calculated elastic parameters of austenitic stainless steels. The maps show the bulk modulus (a) and shear modulus (b) of paramagnetic Fe–Cr–Ni alloys as a function of the Cr and Ni concentrations (balance Fe).

Parametri elastici calcolati per acciai inossidabili austenitici. Le mappe mostrano il modulo di compressibilità (a) e il modulo di taglio (b) delle leghe paramagnetiche Fe–Cr–Ni in funzione delle concentrazioni di Cr e Ni (Fe a bilanciare).

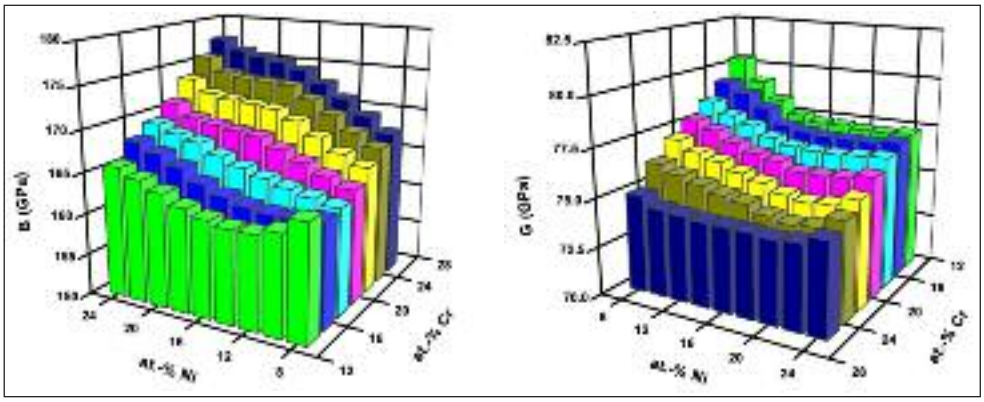

fault energies of steels. For the magnetic contribution to the free energy one may employ models which are more advanced than the mean-field approximation used here (e.g., model, which can take into account the longitudinal spin fluctuations). However, this will not change the general conclusion that local magnetic moments have a marked contribution to the energetic of the stacking faults. Any mechanism (alloying, temperature or strong magnetic field) that can alter the magnetic structure of these alloys is predicted to have large impact on the stacking fault energies and thus on the strength of the paramagnetic Fe-Cr-Ni alloys.

One important implication of the above finding is that the same alloying element can cause totally opposite changes in the SFE of alloys with different host composition, indicating that in practice no universal composition equations for the SFE can be established. To illustrate this effect, in Fig. 4 we show the theoretical room-temperature SFE maps for Fe-Cr-Ni-Mn and Fe-Cr-Ni-Co alloys as a function of composition [32]. It is found that Mn decreases the SFE in alloys with less than 16 at.% Ni, beyond which the SFE slightly rises with Mn. On the other hand, Co always tends to decrease the SFE and the decreasing effect is enhanced in high-Ni alloys. Cobalt is known as a useful alloying element in improving the steel resistance against galling. Enhanced galling effect, in turn, is thought to be associated with enhanced ductility [34]. According to our study (Fig. 4b), Co decreases the SFE and thus decreases the ductility of austenitic stainless steels. This might explain why Co acts as an efficient anti-galling alloying ingredient.

Elastic parameters

The elastic constants are intrinsic properties of a particular crystal structure and thus their alloying and magnetic state dependence may be weaker than that experienced in the case of stacking fault energies. Indeed, our former calculation [12,13] for the polycrystalline elastic moduli (derived from single crystal elastic constants) of paramagnetic fcc Fe-Cr-Ni alloys show weak composition dependence (Fig. 5). Nevertheless, as we will show below, these bulk parameters also exhibit magnetic state dependence and mechanism changing the local magnetic moments within the paramagnetic phase are expected to alter the elastic properties of Fe-Cr-Ni alloys.

We demonstrate the magnetic state dependence of the elastic constants of austenitic stainless steel alloys in the case of $Fe_{0.70}Cr_{0.15}Ni_{0.15}$ alloy by calculating the two single crystal shear elastic constants (c' and c_{44}) as a function of local magnetic moment on Fe sites (μ_{Fe}). The accuracy of our theoretical tool for this particular alloy was established in Ref. [33]. The theoretical equilibrium bulk parameters and the elastic constants for $Fe_{0.70}Cr_{0.15}Ni_{0.15}$ are compared with the available experimental data in Table II. We find ~3.0% mean absolute relative deviation between the theoretical and experimental [35] single-crystal elastic constants. As a matter of fact, this error is much smaller than that obtained for ferromagnetic bcc Fe [15]. The conspicuously better accuracy achieved for Fe-Cr-Ni compared to Fe may be ascribed to the fact that theory gives a highly accurate equation of state for paramagnetic Fe-Cr-Ni: the relative errors in the equilibrium atomic radius and bulk modulus being 0.4% and 1.1%, respectively.

Figure 6a displays the c' and c_{44} elastic constants as a function of μ_{Fe} for spin-constrained calculations (solid lines) and for fully self-consistent calculations (single symbols at $\mu_{Fe} = 1.63\ \mu_B$ corresponding to the self-consistent result). The fact that the fully self-consistent and the spin-constrained results are relatively close to each other is due to the fact that upon lattice distortion the local magnetic moments do not change significantly. This is illustrated in Fig. 6b, where we plotted the local magnetic moment on Fe atoms for the paramagnetic $Fe_{0.80}Cr_{0.15}Ni_{0.05}$ alloy as

TAB. II
Theoretical and experimental [35] equilibrium Wigner-Seitz radius (w_0, in Bohr), bulk modulus (B, in GPa), and single-crystal elastic constants (c_{ij}, in GPa) of paramagnetic fcc $Fe_{0.70}Cr_{0.15}Ni_{0.15}$ alloy. The numbers from the second row are the relative deviations (in %) between the theoretical and the mean experimental values.

	w_0	B	c_{11}	c_{12}	c'	c_{44}
theory	2.66	162.23	203.86	141.42	31.22	133.20
error	0.4	1.1	-2.5	4.0	-14.5	2.5
experiment	2.65	159-162	207-211	135-137	35-38	130

Equilibrio teorico e sperimentale [35] del raggio Wigner-Seitz (w_0, in Bohr), del modulo di compressibilità (B, in GPa), e delle costanti elastiche dei monocristalli (c_{ij}, in GPa) della lega paramagnetica fcc $Fe_{0.70}Cr_{0.15}Ni_{0.15}$. Le cifre della seconda riga sono le deviazioni relative (in %) fra i valori teorici e i valori medi sperimentali.

FIG. 6
a): Single-crystal elastic constants of paramagnetic fcc $Fe_{0.70}Cr_{0.15}Ni_{0.15}$ alloy as a function of the local magnetic moment on the Fe atoms. Note that c' has been multiplied by three in order to match its scale to that of c_{44}. Shown are also the floating spin results obtained at the equilibrium magnetic moment μ_{Fe} = 1.63 μ_B (separate circle and square). All calculations were performed at paramagnetic volume (w=2.66 Bohr). b): local magnetic moments on Fe atoms of paramagnetic $Fe_{0.80}Cr_{0.15}Ni_{0.05}$ alloy as a function of Wigner-Seitz radius w and tetragonal lattice parameter ratio c/a.

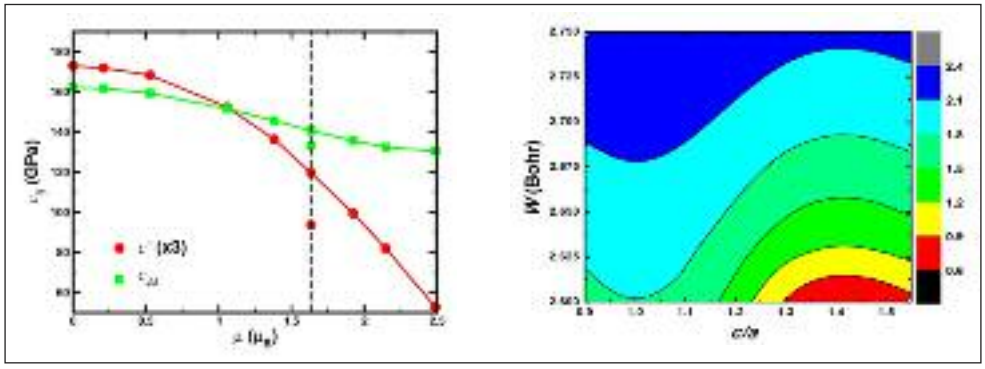

a): Costanti elastiche di monocristalli della lega paramagnetica fcc $Fe_{0.70}Cr_{0.15}Ni_{0.15}$ in funzione del momento magnetico locale sugli atomi di Fe. Si noti che c' è stata moltiplicata per 3 per far corrispondere la scala a quella di c_{44}. Vengono mostrati anche i risultati di floating spin ottenuti al momento magnetico locale μ_{Fe} = 1.63 μ_B (cerchio e quadrato separati). Tutti I calcoli sono stati eseguiti al volume paramagnetico (w=2.66 Bohr). b): momenti magnetici locali sugli atomi di Fe della lega paramagnetica $Fe_{0.80}Cr_{0.15}Ni_{0.05}$ in funzione di raggio Wigner-Seitz w e rapporto del parametro del reticolo tetragonale c/a.

a function of volume (Wigner-Seitz radius, w) and tetragonal lattice constant ratio c/a. The theoretical equilibrium w for the fcc phase is 2.66 Bohr, and for the body centred cubic (bcc) phase is 2.68 Bohr. We recall that the fcc structure has c/a ≈ 1.41 and the c' elastic constant is proportional with the curvature of the total energy versus c/a (for fixed volume). It is interesting to note that the local magnetic moments slightly increase upon tetragonal lattice distortion in the fcc phase (c/a≈1.41) and decrease in the bcc phase (c/a=1.0).

Returning to Fig. 6a, we observe that both elastic constants strongly depend on the local magnetic moment. The effect is somewhat more pronounced for the tetragonal elastic constant. From a polynomial fit to the data from Fig. 6a, for the slopes of the elastic constants versus magnetic moment we obtain $\delta c'/\delta\mu \approx -22.5$ GPa/μ_B and $\delta c_{44}/\delta\mu \approx -19.5$ GPa/μ_B. Hence, 0.1μ_B change in the local magnetic moment results in ~2 GPa change in the elastic constants, representing ~6% for c' and ~2% for c_{44}. This is an important effect, especially taking into account that we are dealing with a system well above its magnetic transition temperature. We suggest that by manipulating the magnetism, e.g., via chemical composition, chemical ordering, external field, or temperature, one is able to tailor the thermo-elastic properties of austenitic stainless steels. We have demonstrated the above effect in the case of the temperature dependence of the single-crystal elastic constants of paramagnetic Fe-Cr-Ni alloys [33]. In particular, we have shown that spin fluctuation in paramagnetic Fe-Cr-Ni alloys can account for 63% of $\delta c'/\delta T$ and 28% for $\delta c_{44}/\delta T$ as compared to the experimental measurements [35].

So far we considered concentrated random alloys and investigated the impact of magnetism on their bulk parameters. One may ask what happens in dilute alloys, how the elastic constants and the corresponding elastic and size misfit parameters (and thus the solid solution hardening effects) are influenced by the magnetic state. In order to answer this question one should perform a series of self-consistent total energy calculation for paramagnetic and ferromagnetic alloys and extract the magnetic state dependence of the elastic properties. In lack of such data, in Fig. 7 we compare the single crystal and polycrystalline elastic parameters of Fe-Cr and Fe-Co alloys calculated for fcc and bcc phases as a function of composition. In these calculations the bcc phase was assumed to be ferromagnetic and the fcc phase paramagnetic. See Refs. [14-16] for a detailed comparison between the theoretical and experimental elastic parameters for binary Fe-based alloys.

We find that the paramagnetic fcc alloys have significantly smaller tetragonal elastic constant c' than the ferromagnetic bcc alloys. At the same time, c_{44} is larger in the fcc phase than in the bcc one. Alloying has a rather small effect on the scale from Fig. 7 (upper panel). Therefore, we can conclude that the ferromagnetic bcc Fe-based alloys are more isotropic than the paramagnetic fcc counterparts, and this difference to a large extent is due to the soft tetragonal mode in the paramagnetic fcc phase.

All polycrystalline elastic moduli are smaller in the fcc phase compared to the bcc phase because of the rather small c' in the fcc phase, However, the compositional changes are rather important when comparing the fcc and bcc elastic moduli. The bulk modulus B, shear modulus G, and Young's modulus E of the paramagnetic fcc Fe increase slightly as a function of Co content.

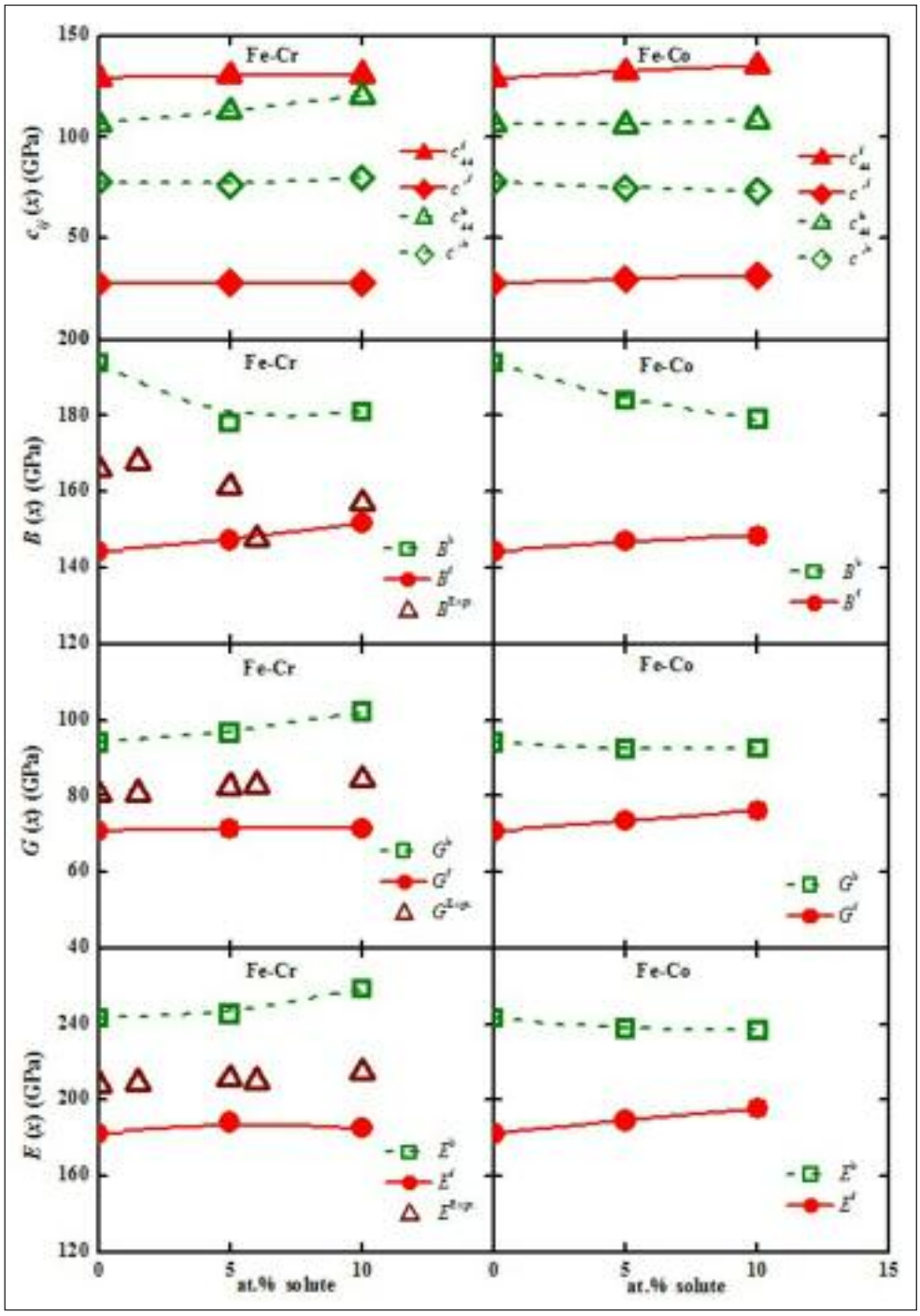

FIG. 7
Single crystal and polycrystalline elastic parameters of paramagnetic fcc Fe-Cr and Fe-Co alloys (red circles) and of ferromagnetic bcc Fe-Cr and Fe-Co alloys (green squares) plotted as a function of Co or Cr content. The superscripts ^{f} and ^{b} stand for the fcc and bcc phases, respectively. Shown are the two single crystal shear elastic constants c' and c_{44}, the bulk modulus B, the shear modulus G and the Young's modulus E. For ferromagnetic bcc Fe-Cr the available experimental polycrystalline elastic parameters [5] are also shown (brown triangles).

Parametri elastici di cristallo singolo e policristallini di leghe paramagnetiche fcc Fe-Cr e Fe-Co (cerchi rossi) e di leghe ferromagnetiche bcc Fe-Cr e Fe-Co (quadrati verdi) tracciati in funzione del contenuto di Co o Cr. Gli apici ^{f} e ^{b} corrispondono rispettivamente alle fasi fcc e bcc. Sono mostrate le due costanti elastiche di taglio dei due monocristalli c' e c_{44}, il modulo di compressibilità B, il modulo di taglio G e il modulo di Young E. Sono mostrati anche (triangoli marroni) i parametri elastici policristallini [5] sperimentali disponibili per la lega ferromagnetica bcc Fe-Cr.

In the fcc phase, both Co and Cr show relatively small impact on the elastic parameters and the alloying effects are more pronounced in the ferromagnetic bcc phase. However, in order to see where this stronger effect comes from, one should carry out similar calculations for the paramagnetic bcc alloys to be able to exclude the effect of crystal lattice from the above comparison.

Bain path of paramagnetic Fe-Cr and Fe-Cr-Ni alloys

The transformation mechanism between the bcc and the fcc phases of Fe-based alloys is of key importance for the properties of alloy steels. This is a typical diffusionless structural change belonging to the group of the so called martensitic transformations. Several homogeneous paths have been suggested for describing the bcc-fcc transformation. In particular, the Bain path is obtained by expanding the bcc lattice along one of the cubic axes (c) and contracting along the two others (a). Upon lattice deformation the crystal symmetry remains tetragonal and the unit cell is body centered tetragonal (bct). The tetragonality of the lattice is described by the c/a ratio. When c/a is 1 the bct lattice corresponds to the bcc one, whereas when c/a reaches $\sqrt{2}$ the bct lattice turns into the fcc one. The Bain path is an appropriate model for studying the energetics of the bcc-fcc martensitic transformation. Furthermore, monitoring the alloying-induced softening or hardening of Fe-based alloys against tetragonal distortions [36] is of key importance for understanding the interstitial driven martensitic transformations in alloy steels.

In Fig. 8, we present the calculated total energy maps for Fe-Cr and Fe-Cr-Ni alloys along with the Bain path. The energy map for $Fe_{0.90}Cr_{0.10}$ (Fig. 8a) shows that at the equilibrium volume the close-packed fcc structure is marginally more stable than the

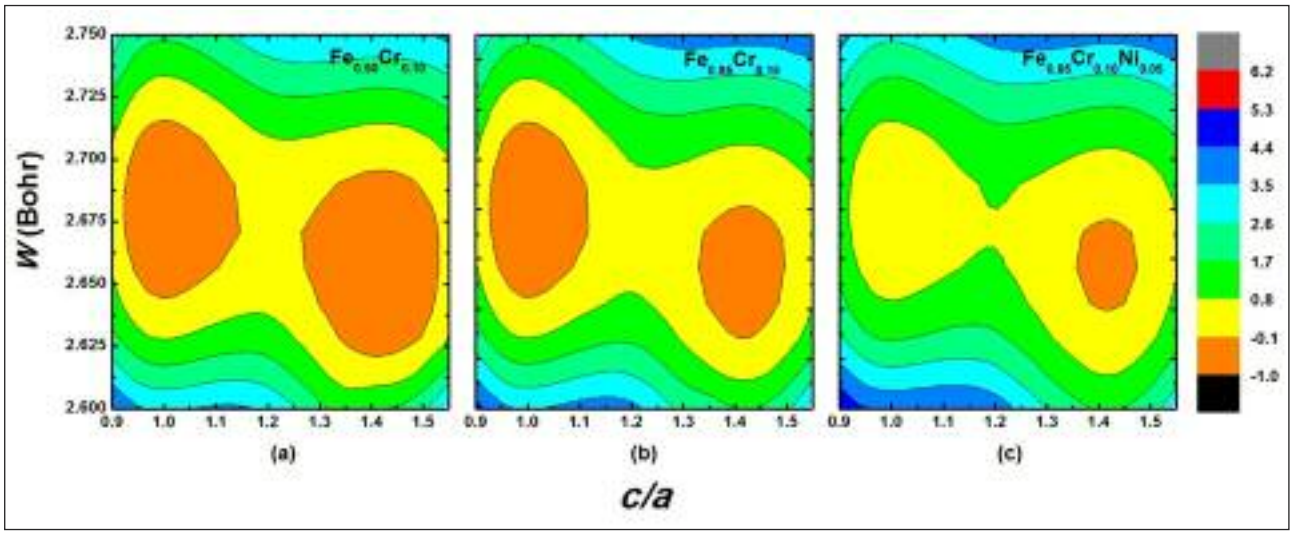

FIG. 8 ***Total energy contours (in mRy) for (a) $Fe_{0.9}Cr_{0.1}$, (b) $Fe_{0.85}Cr_{0.15}$ and (c) $Fe_{0.85}Cr_{0.1}Ni_{0.05}$ alloys as a function of the tetragonal lattice ratio (c/a) and the Wigner-Seitz radius (w). For each alloy, the energies are plotted relative to the minimum of the corresponding bcc (c/a = $(c/a)_{bcc}$ = 1) total energy.***

Profili dell'energia totale (in mRy) per leghe (a) $Fe_{0.9}Cr_{0.1}$, (b) $Fe_{0.85}Cr_{0.15}$ e (c) $Fe_{0.85}Cr_{0.1}Ni_{0.05}$ in funzione del rapporto del reticolo tetragonale (c/a) e del raggio di Wigner-Seitz (w). Per ogni lega sono tracciate le energie relative al minimo della corrispondente energia tolale bcc (c/a = $(c/a)_{bcc}$ = 1).

bcc modification, the energy differences between the fcc and the bcc structures being $\Delta E \equiv E_{fcc} - E_{bcc}$ = -0.021 mRy. There is a clear energy barrier, a saddle point between the bcc and fcc local minima. Approximating the energy barrier by the total energy calculated for c/a =1.2 and w = 2.675 Bohr, for $Fe_{0.9}Cr_{0.1}$ we obtain $\Delta E_f \equiv E_{1.2} - E_{fcc}$ = 1.019 mRy (barrier relative to the fcc structure) or $\Delta E_b \equiv E_{1.2} - E_{bcc}$ = 0.998 mRy (barrier relative to the bcc structure). Obviously $\Delta E_b - \Delta E_f = \Delta E$.

Since in the present calculations no temperature effects are taken into account (except the chemical and magnetic randomness in the total energy) the total energy difference ΔE between the fcc and bcc structures should be interpreted with precaution and should not be associated with the phase stability of Fe-Cr alloys. Nevertheless, we can make our conclusions more robust and identify the primary chemical effects on the phase stability by considering the $Fe_{0.90}Cr_{0.10}$ as reference and focus on the total energy of $Fe_{0.85}Cr_{0.1}M_{0.05}$ (M stands for Cr and Ni) expressed relative to that calculated for $Fe_{0.90}Cr_{0.10}$. The corresponding relative fcc-bcc energy difference is denoted by ΔE(M) and the relative energy barriers by ΔE_f(M) or ΔE_b(M). According to this definition, for instance vanishing ΔE(M) and $\Delta E_{f/b}$(M) mean that 5 % alloying addition M produces negligible effect on the corresponding energy differences of $Fe_{0.9}Cr_{0.1}$.

Next, we illustrate the effect of adding 5% Cr and Ni on the Bain path of the paramagnetic Fe-Cr alloy. We find that adding 5 % Cr to the $Fe_{0.9}Cr_{0.1}$ alloy increases the fcc-bcc total energy difference by ΔE(Cr) = 0.443 mRy (Fig. 8b). In other words, the chemical effect of Cr is to stabilize the bcc phase relative to the fcc one. Alloying changes the energy barrier between the bcc and fcc structures as well. We obtain that 5 % Cr addition to $Fe_{0.9}Cr_{0.1}$ alters the barrier by ΔE_f(Cr) = -0.118 mRy or ΔE_b(Cr) = 0.325 mRy. That is, the energy minimum around the fcc phase becomes shallower and that around the bcc phase deeper by alloying with Cr. In terms of mechanical stability of alloys, the above alloying effect of Cr corresponds to mechanically less (more) stable fcc (bcc) phase. This is in line with the observation that Cr decreases the tetragonal elastic constant of paramagnetic fcc $Fe_{0.9}$Cr0.1.

Nickel is calculated to have pronounced effects on the Bain path of paramagnetic Fe-Cr alloys (Fig. 8c). Adding 5 % Ni to $Fe_{0.9}Cr_{0.1}$ yields ΔE(Ni) = -0.300 mRy and changes the energy barrier by ΔE_f(Ni) = 0.045 mRy per atom or ΔE_b(Ni) = -0.255 mRy per atom relative to that of $Fe_{0.9}Cr_{0.1}$. It is interesting to contrast the above trends for the energy barrier with those calculated for the elastic constants of paramagnetic fcc Fe alloys. In particular, Ni is predicted to decrease the tetragonal elastic constant of fcc Fe. Thus we may conclude that the trends in the elastic constants are not sufficient to predict the changes in the energy barrier upon alloying.

CONCLUSIONS

Magneto-elastic phenomena in magnetic materials and, in particular, in alloy steels have been known for a long time. However, the magnetic effects on the stacking fault energies and elastic constants of magnetic materials in their paramagnetic state have been less well documented. In this work, using first-principles computational methods, we have investigated the atomic-scale chemical, magnetic and structural effects behind the stacking fault energies and elastic properties of paramagnetic Fe-Cr-Ni alloys. We have demonstrated that in this important class of "nonmagnetic" engineering materials, magnetism gives a major contribution to the fundamental bulk properties.

ACKNOWLEDGMENTS

The Swedish Research Council, the Swedish Steel Producers' Association (Jernkontoret), the Swedish Foundation for Strategic Research, the China Scholarship Council, the Erasmus Mundus External Cooperation Lot3, and the Hungarian Academy of Sciences (research project OTKA 84078) are acknowledged for financial support.

REFERENCES

1. MRS Fall meeting 2010. Symposium New Methods in Steel Design – Steel Ab initio (www.mrs.org/meetings).
2. G. WRANGLEN, An Introduction to Corrosion and Protection of Metals. Chapman and Hall, New York (1985).

3. C. W. LUGN and N. H. MARCH, Mechanical Properties of Metals. World Scientific Publishing Co. Pte. Ltd. (1999).
4. R. L. FLEISCHER, Acta Met. 11, (1963), p.203; R. LABUSCH, Acta Met. 20, (1972), p.917; F. R. N. NABARRO, Phil. Mag. 35, (1977), p.613.
5. G. R. SPEICH, A. J. SCHWOEBLE and W. C. LESLIE, Metall. Trans. 3, (1972), p.2031.
6. G. GHOSH and G. B. OLSON, Acta Mater. 50, (2002), p.2655.
7. L. VITOS, P. A. KORZHAVYI, J.-O. NILSSON and B. JOHANSSON, Physica Scripta 77, (2008), p.065703 and references therein.
8. K. ISHIDA, Phys. Status Solidi (a) 36, (1976), p.717.
9. G. GRIMVALL, Phys. Scr. 13, (1976), p.59.
10. L. VITOS, P. A. KORZHAVYI, and B. JOHANSSON, Phys. Rev. Lett. 96, (2006), p.117210.
11. L. VITOS, J.-O. NILSSON and B. JOHANSSON, Acta Mater. 54, (2006), p.3821.
12. L. VITOS, P. A. KORZHAVYI, and B. JOHANSSON, Nature Mater. 2, (2003), p.25.
13. L. VITOS, P. A. KORZHAVYI, and B. JOHANSSON, Phys. Rev. Lett. 88, (2002), p.155501.
14. H. L. ZHANG, B. JOHANSSON and L. VITOS, Phys. Rev. B 79, (2009), p.224201.
15. H. L. ZHANG, M. P. J. PUNKKINEN, B. JOHANSSON, S. HERTZMAN, and L. VITOS, Phys. Rev. B 81, (2010), p.184105.
16. H. L. ZHANG, M. P. J. PUNKKINEN, B. JOHANSSON, and L. VITOS, J. Phys.: Condens. Matter 22, (2010), p.275402.
17. O. K. ANDERSEN, O. JEPSEN, and G. KRIER, in Lectures on Methods of Electronic Structure Calculations, edited by V. KUMAR, O. K. ANDERSEN, and A. MOOKERJEE, World Scientific Publishing Co., Singapore, (1994), p.63.
18. L. VITOS, Phys. Rev. B 64, 014107 (2001).
19. L. VITOS, Computational Quantum Mechanics for Materials Engineers: The EMTO Method and Applications. Springer-Verlag London, Series: Engineering Materials and Processes (2007).
20. P. HOHENBERG and W. KOHN, Phys. Rev. 136, (1964), p.B864.
21. J. KOLLÁR, L. VITOS and H. L. SKRIVER, in Electronic Structure and Physical Properties of Solids: the Uses of the LMTO Method, Lectures Notes in Physics, edited by H. DREYSSE, Springer-Verlag, Berlin, (2000), p. 85.
22. L. VITOS, I. A. ABRIKOSOV and B. JOHANSSON, Phys. Rev. Lett. 87, (2001), p.156401.
23. P. SOVEN, Phys. Rev. 156, (1967), p.809; B. L. GYÖRFFY, Phys. Rev. B 5, (1972), p.2382.
24. J. P. PERDEW, K. BURKE and M. ERNZERHOF, Phys. Rev. Lett. 77, (1996), p.3865.
25. B. L. GYÖRFFY, A. J. PINDOR, G. M. STOCKS, J. STAUNTON, and H. WINTER, J. Phys. F 15, (1985), p.1337.
26. B. MAGYARI-KÖPE, L. VITOS and G. GRIMVALL, Phys. Rev. B 70, (2004), p.052102.
27. A. TAGA, L. VITOS, B. JOHANSSON and G. GRIMVALL, Phys. Rev. B 71, (2005), p.014201.
28. M. ROPO, K. KOKKO, L. VITOS and J. KOLLÁR, Phys. Rev. B 71, (2005), p.045411.
29. E. K. DELCZEG-CZIRJAK, L. DELCZEG, M. ROPO, K. KOKKO, M. P. J. PUNKKINEN, B. JOHANSSON and L. VITOS, Phys. Rev. B 79, (2009), p.085107.
30. B. MAGYARI-KÖPE, L. VITOS, B. JOHANSSON and J. B. KOLLÁR, Acta Cryst. B57, (2001), p.491.
31. B. MAGYARI-KÖPE, L. VITOS, G. GRIMVALL, B. JOHANSSON and J. B. KOLLÁR, Phys. Rev. B 65, (2002), p.193107.
32. S. LU, Q.-M. HU, B. JOHANSSON, L. VITOS, Acta Materialia 59, (2011), p.5728.
33. L. VITOS and B. JOHANSSON, Phys. Rev. B. 79, (2009), p.024415.
34. ASM SPECIALTY HANDBOOK: STAINLESS STEELS (DAVIS AND ASSOCIATES, MATERIALS PARK, OH, 1994).
35. A. TEKLU, H. LEDBETTER, S. KIM, L. A. BOATNER, M. McGUIRE and V. KEPPENS, Metall. Mater. Trans. A 35, (2004), p.024415.
36. N. AL-ZOUBI, B. JOHANSSON, G. NILSON, and L. VITOS, J. Journal of Applied Physics 110, (2011), p.013708.

Abstract

Leghe di acciaio inossidabile dalla teoria dei principi primi

Parole chiave: Acciaio inossidabile, proprietà, modellazione

Ottenere una descrizione accurata dei materiali richiede, ovviamente, le più avanzate tecniche su scala atomica di entrambe le aree: sperimentale e teorica. Tuttavia, nonostante il gran numero di tecniche disponibili, lo studio sperimentale di caratteristiche e fenomeni su scala atomica è piuttosto difficile anche in solidi semplici. Negli acciai le sfide diventano più complesse a causa dell' interazione tra gli effetti strutturali, chimici e magnetici. D'altro canto, metodi avanzati computazionali basati sulla teoria DFT - Density Functional Theory, garantiscono una base adeguata per studiare le proprietà fondamentali dei materiali di acciaio dai principi primi. Il nostro gruppo del Royal Institute of Technology di Stoccolma ha un ruolo a livello internazionale nello sviluppo e nell'applicazione di codici di calcolo per tali applicazioni. Utilizzando i nostri strumenti ab initio, abbiamo presentato una panoramica della struttura elettronica e magnetica, e le caratteristiche micromeccaniche delle leghe di acciaio inossidabile austenitico. Nel presente studio, vengono passati in rassegna gli sviluppi più importanti relativi alla progettazione ab initio dell'acciaio, assistita dalla meccanica quantistica, con particolare enfasi per il ruolo del magnetismo sulle caratteristiche fondamentali degli acciai legati.